Supporting Information

Magneto-mechanical Actuation of Magnetic Responsive Fibrous Scaffolds Boosts Tenogenesis of Human Adipose Stem Cells

Ana R. Tomás, Ana I. Gonçalves, Elvira Paz, Paulo Freitas, Rui M. A. Domingues, Manuela E. Gomes**

1. Supplementary Results

1.1. Magnetic nanoparticles characterization

1.1.1. FTIR Spectroscopy

Fourier Transform Infrared (FTIR) Spectroscopy was used to assess the chemical composition of MNP@CNC (Fig. S1). MNP@CNC spectrum exhibited characteristic peaks of cellulose, appearing at 3347 and 2900 cm^{-1} (–OH and –CH stretching, respectively), 1163 cm^{-1} (C-O-C stretching), 1113, 1059 and 1034 cm^{-1} (C-OH stretching),[1] and of iron oxide, at 583 cm^{-1} corresponding to the Fe-O vibrational frequencies,[2] confirming the formation of iron oxide nanoparticles on the CNCs surface (Fig. S1).

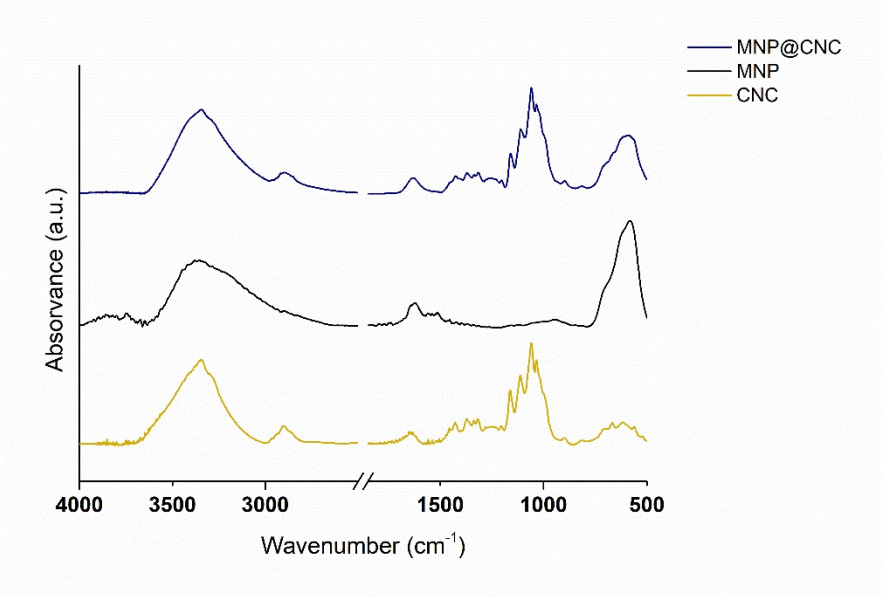

Fig. S1. FTIR spectra of neat CNCs, MNPs and MNP@CNC.

1.1.2. X-Ray Diffraction (XRD)

The crystalline phase of the nanoparticles was assessed through X-Ray Diffraction (XRD) (Fig. S2). The CNCs diffractogram shows characteristic peaks at 2θ = 15.4°, 15.9°, 22.7° corresponding to the 1-10, 110 and 200 crystalline reflection planes, respectively. [1] The MNP@CNC diffractograms are dominated by the characteristic peaks of magnetite (Fe_3O_4) nanoparticles at 2θ = 30.2°, 35.7°, 43.3°, 53.7°, 57.3°, 62.8°, corresponding to the (220), (311), (400), (422), (511) and (440) reflection planes respectively,[1] along with the highest intensity peak of CNC at 22.7°, confirming the presence of iron oxide MNPS on the CNCs surface. On the other hand, the diffractogram of coated MNP@CNC exhibit a similar pattern to that of bare MNP@CNC which indicates that the coating strategies did not impact the nanoparticles crystallinity. Additionally, the crystallite size of the anchored MNPs was calculated through Scherrer's equation,[3] from which the estimated MNPs size was 7.41 ± 0.45 nm of diameter (Table S1).

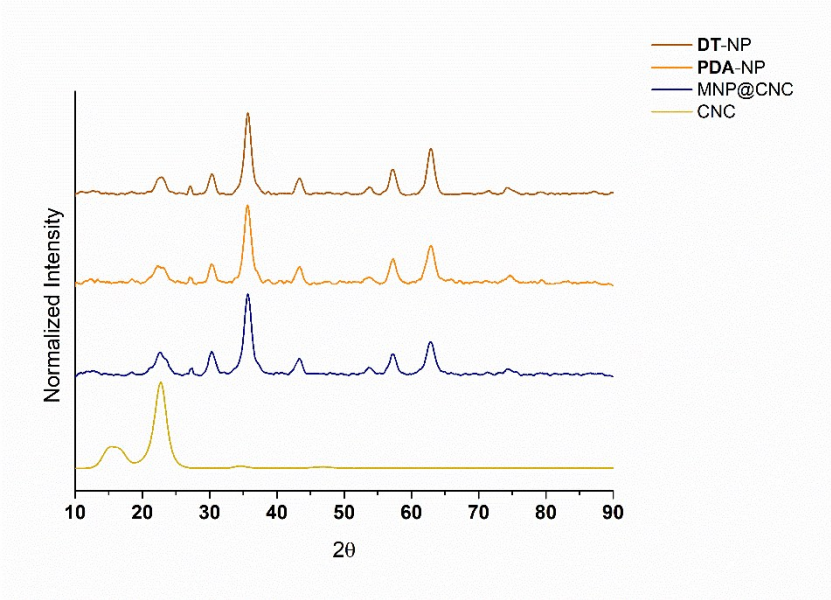

Fig. S2. XRD spectra of CNC, MNP@CNC, PDA-NP and DT-NP.

Table S1. Iron oxide nanoparticle crystallite size and respective measurements from the XRD spectra

Sample	Reflection plane	Peak position 2θ (°)	FWHM 2θ (°)	Crystallite size (nm)
MNP@CNC	311	35.7	1.25	6.96
	440	62.8	1.38	7.00
PDA-NP	311	35.7	1.17	7.46
	440	62.9	1.37	7.06
DT-NP	311	35.7	1.12	7.81
	440	62.9	1.19	8.18

presented in Fig. S2.

1.1.3. Thermogravimetric Analysis (TGA)

Thermogravimetric Analysis (TGA) was performed to evaluate the amount of MNPs adsorbed onto the CNCs (Fig. S3). The CNC degradation profile translates their organic nature, showing that the sample was fully degraded, with 0.36 % of the initial mass remaining after analysis. On the other hand, the MNP@CNC degradation profile shows superior thermal stability compared to that of CNCs due to the incorporation of iron oxide nanoparticles, which are thermodynamically stable at temperatures superior to 570 °C. [1,2] Thus, the content

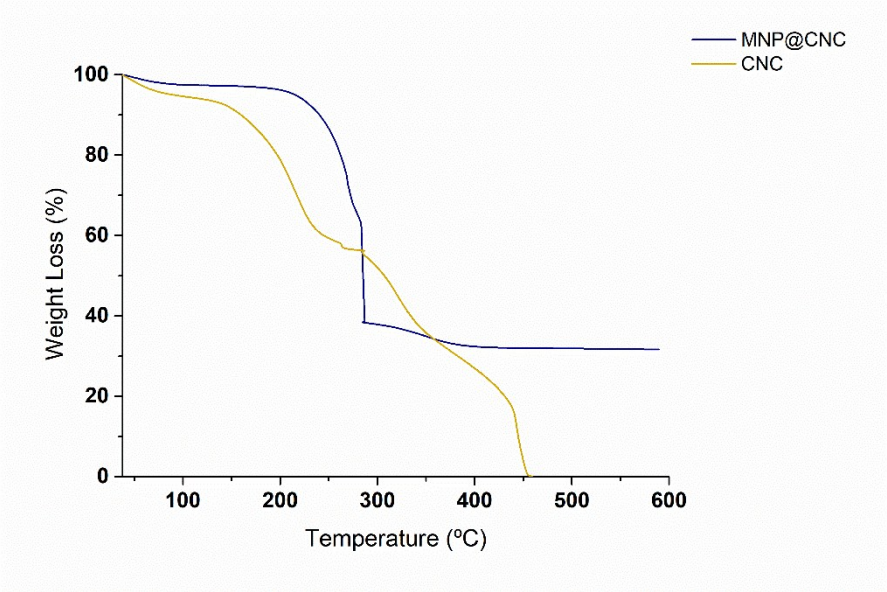

of magnetic material in MNP@CNC was estimated to be 32.4 wt.%, considering the remaining weight of the sample consists only in inorganic material.

Fig. S3. TGA thermograph of CNCs and MNP@CNC.

1.2. Characterization of electrospun fibrous constructs

1.2.4. Thread and Fiber Diameters

Nanofiller content and take-up speed were optimized to minimize the threads diameter without compromising their mechanical and magnetic properties. The variation of the constructs' diameters with the increase in nanofiller content and in take-up speed are shown in Fig. S4 and S5, respectively, and summarized in Table S2.

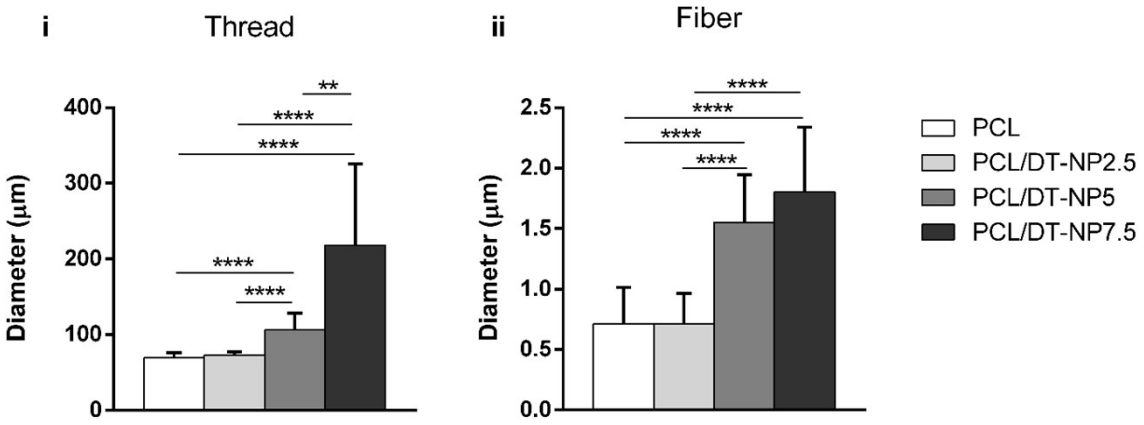

Fig. S4. Variation of the diameter of PCL threads (i) and respective fibers (ii) with the increase in nanofiller content (**p ≤ 0.01****p ≤ 0.0001).

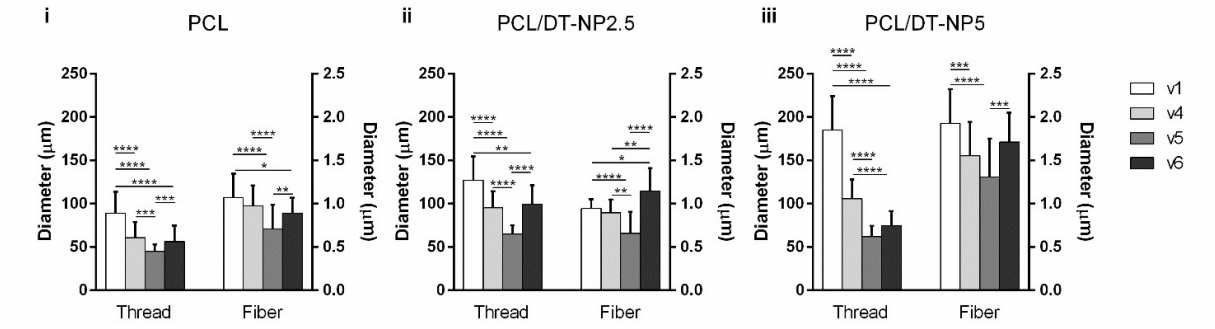

Fig. S5. Variation of the diameter of PCL threads with 0 % (i), 2.5 % (ii) and 5 % (iii) DT-NP and of the respective fibers with the increase in the constructs take-up speed (*p≤ 0.05 **p ≤ 0.01***p≤ 0.001 ****p ≤ 0.0001). Tested speeds were 0.24 cm s^{-1} (v1), 0.56 cm s^{-1} (v4), 0.73 cm s^{-1} (v5) and 0.86 cm s^{-1} (v6).

Table S2. Influence of the nanofiller content and take-up speed on the thread and fiber diameters of PCL threads. Tested speeds were 0.24 cm s^{-1} (v1), 0.56 cm s^{-1} (v4), 0.73 cm s^{-1} (v5) and 0.86 cm s^{-1} (v6).

Nanofiller Content	Diameter (μm)							
	Thread				Fiber			
	v1	v4	v5	v6	v1	v4	v5	v6
PCL	89.22 ± 24.46	60.81 ± 18.28	44.85 ± 8.34	56.26 ± 18.69	1.07 ± 0.28	0.97 ± 0.24	0.71 ± 0.28	0.89 ± 0.18
PCL/DT-NP2.5	127.24 ± 27.37	95.37 ± 18.88	65.13 ± 10.09	99.46 ± 21.79	0.95 ± 0.11	0.90 ± 0.15	0.66 ± 0.25	1.15 ± 0.27
PCL/DT-NP5	184.88 ± 39.52	106.03 ± 22.16	62.01 ± 12.39	74.53 ± 16.86	1.93 ± 0.39	1.55 ± 0.39	1.31 ± 0.45	1.71 ± 0.34

1.2.5. Fiber Alignment

Fiber alignment was evaluated on SEM images of PCL/DT-NP5 (Fig. S6). For this purpose, directionality histograms of fibers of each condition were calculated and one of each is presented in Fig. S6A for comparison. To quantify the differences between spectra of different conditions, the respective peaks were fitted with a Gaussian function, and the average FWHM and height were compared in Fig. S6B.

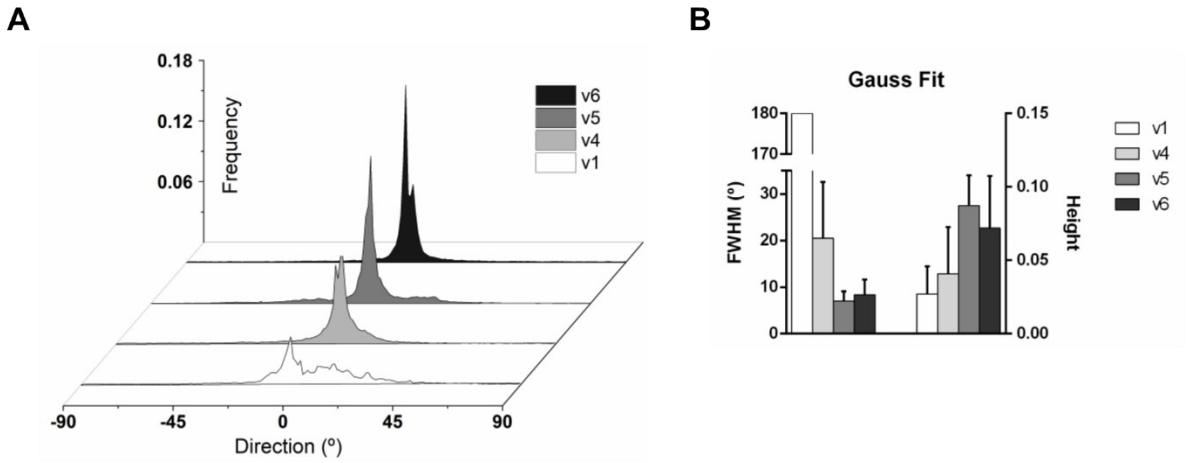

Fig. S6. Analysis of fiber alignment in threads fabricated at different take up speeds. (A) Directionality spectra of SEM images of PCL/DT-NP5 threads fabricated at different take-up speeds. (B) Comparison between their peaks dimensions (FWHM and Height), obtained after Gaussian fitting of the spectra from each condition (n=3). Tested speeds were 0.24 cm s^{-1} (v1), 0.56 cm s^{-1} (v4), 0.73 cm s^{-1} (v5) and 0.86 cm s^{-1} (v6).

1.2.6. Mechanical Properties

The influence of the increase in nanofiller content on the yarns mechanical properties are summarized in Table S3.

Table S3. Influence of nanofiller content on the yarns mechanical properties.

	Young's Modulus (MPa)	Yield Strength (MPa)	Yield Strain ($mm.mm^{-1}$)	Strain at Break ($mm.mm^{-1}$)	Ultimate Tensile Strength (MPa)
PCL	12.10 ± 1.26	1.41 ± 0.12	0.17 ± 0.01	3.44 ± 0.68	2.90 ± 0.41
PCL/DT-NP2.5	17.92 ± 2.18	1.77 ± 0.18	0.15 ± 0.01	3.84 ± 0.38	4.07 ± 0.40
PCL/DT-NP5	21.55 ± 4.91	2.22 ± 0.30	0.16 ± 0.01	4.22 ± 0.52	4.70 ± 0.53

2. Supplementary Methods

2.1. Synthesis of CNCs

Cellulose nanocrystals (CNCs) were produced through sulfuric acid hydrolysis of MCC, according to Bondeson *et al.*, 2006 [4] and Domingues *et al.,* 2016 [5] and adapted according to the reports from Chen *et al.*, 2015.[6] Hydrolysis was performed with 62 wt.% sulfuric acid at 60 °C for 40 minutes under mechanical stirring. The reaction was stopped by adding fivefold of cold deionized (DI) water, the resulting suspension decanted and subsequently washed through repeated centrifugation cycles (9000 rpm, 5ºC, 10 min $cycle^{-1}$), until the supernatant became turbid. Then, the CNC suspension was collected and dialyzed (cellulose dialysis tubing membranes, MWCO: 12-14 kDa, 0-76 mm width, Sigma-Aldrich, France) for 7 days, against DI water until neutral pH. The membranes content was subjected to 5 sonication cycles (ultrasonic processor, VCX-130PB-220, Sonics, USA, 5 min $cycle^{-1}$), using an ultrasound probe (Horn ½" SOLID vc 70/13c 3 – 0561) at 60 % of amplitude output, under ice cooling to prevent overheating. The CNC suspension was then centrifuged (9000 rpm, 5ºC, 10 min $cycle^{-1}$) to remove big particles and stored at 4 °C until further use.

2.2. Production of MNP@CNC

MNP@CNC were produced through co-precipitation of Fe^{2+} and Fe^{3+} with ammonium hydroxide in the presence of CNCs and under N_2 environment to prevent magnetite (Fe_3O_4) oxidation.[7] First, 0.3 % CNC aqueous suspension was placed in a triple bottleneck flask at 70 ºC and under continuous N_2 purging. MNP salt precursors, $FeCl_3 \cdot 6H_2O$ and $FeCl_2 \cdot 4H_2O$ (12mM, 2/1 molar ratio of Fe^{3+}/Fe^{2+}), were dissolved in ultrapure water and added to the CNC suspension, which was then left under vigorous stirring for 2 h. Co-precipitation of Fe^{2+} and Fe^{3+} was induced by adding twofold of 3 % (v/v) ammonium hydroxide solution, with the resulting suspension turned black immediately upon MNP formation. After 1 h under vigorous stirring, MNP@CNC were magnetically separated using a permanent neodymium magnet (DX=X=_N52, K&J Magnetics, USA) and subjected to several washing and centrifugation cycles (9000 rpm, 5ºC, 10 min $cycle^{-1}$) against DI water until neutral pH was achieved. Finally, MNP@CNC were dispersed in ultrapure water and stored at 4 ºC until further use.

2.3. MNP@CNC surface modification

MNP@CNC were coated with PDA following the procedure described on Shi *et al.*, 2015.[8] Previously prepared MNP@CNC were dispersed in tris buffer solution (0.2% final concentration). Tris buffer solution (10 mM, pH 8.5) was prepared by dissolving tris((hydroxyethyl)aminomethane) in ultrapure water and adjusting the pH with an HCl solution. The resulting suspension was sonicated (ultrasonic processor, VCX-130PB-220, Sonics, USA, 1 min cycle^{-1}) using an ultrasound probe (Horn ½" SOLID vc 70/13c 3 – 0561, 40% amplitude output). 2 mg mL^{-1} of dopamine hydrochloride were added to the MNP@CNC suspension, which was then placed in an ultrasonic bath for 5 minutes to promote the homogenous dispersion of dopamine hydrochloride. The MNP@CNC/dopamine hydrochloride suspension was left stirring overnight, in an opened container and at room temperature. Polydopamine coated MNP@CNC (PDA-NP) were collected through magnetic separation using a permanent neodymium magnet (DX=X=_N52, K&J Magnetics, USA) and subjected to several washing and centrifugation cycles (9000 rpm, 5 °C, 20 min cycle^{-1}) against DI water until neutral pH was achieved. PDA-NP were dispersed in ultrapure water and stored at 4 ºC until further use.

PDA-NP surface was further modified with 1-DT adapting the procedure described by Lee *et al.,* 2007.[9] Previously prepared PDA-NP were dispersed in absolute ethanol solution (0.2% final concentration). The resulting suspension was sonicated (ultrasonic processor, VCX-130PB-220, Sonics, USA, 2 min cycle^{-1}) using an ultrasound probe (Horn ½" SOLID vc 70/13c 3 – 0561, 40% amplitude output). After bubbling with N_2, 20 mM of 1-DT and then 10 mM triethylamine, final concentration, were added to the PDA-NP suspension, which was left stirring overnight, in a closed container and at room temperature. 1-DT coated PDA-NP (DT-NP) were subjected to several washing and centrifugation cycles (9000 rpm, 5 °C,

20 min cycle^{-1}) against ethanol and finally dispersed in DMF solution and stored at 4 ºC until further use.

2.4. XRD

The crystallinity of the produced nanoparticles, namely CNCs, MNP@CNC, PDA-NP and DT-NP, was evaluated by acquiring x-ray diffractometry profiles (XRD, Bruker D8 Advance, Bruker, Germany) of 20 mg freeze-dried nanoparticle pellets, over the 2θ range of 10-90° (0.05° scanning step, 2 seconds per step), at 40 kV and 40 mA with a Cu Kα X-ray source. The average crystallite size of the iron oxide MNPs was calculated according to the Scherrer equation[3] (Equation 1) in which, where D_{hkl} is the crystallite size, according to the reflection planes (hkl), K represents the shape factor, here assumed as 0.9, ʎ is the X-Rays wavelength (1.541Å for Cu Kα radiation), Θ is the Bragg's diffraction angle, and β is the full width at half maximum (FWHM) peak intensity.

$$D_{hkl} = \frac{K}{\beta \cos\theta} \quad (1)$$

2.5. TGA

Thermogravimetric Analysis (TGA, Simultaneous Thermal Analyzer, Hitachi, Japan) was performed in freeze dried samples of CNCs and MNP@CNCs to assess the amount of iron oxide MNPs in MNP@CNCs. Samples were subjected to temperatures within a range of 40-600 °C, at a heating rate of 10 °C/min, using crucibles of platinum as a support, under 1:7 oxygen/nitrogen atmosphere with a flow rate of 200 mL min^{-1}. Sample weight at 105 °C (after residual moisture evaporation) was taken as reference for residual mass calculation after thermal degradation.

2.6. Real-time RT-PCR

Total RNA was extracted from the constructs using RiboZol™ RNA Extraction Reagent (N580, VWR) according to the manufacturer's instructions. Briefly, after homogenization/lysis, chloroform (Sigma Aldrich) was added to samples and centrifuged at 12,000 g for 15 minutes at 4 °C, for separation of phases. The upper (aqueous) phase was collected to a new tube for precipitation of RNA by adding isopropanol (Sigma Aldrich) reagent. After 10 minutes of incubation at RT, the samples were centrifuged for 10 minutes at 12,000 x g. RNA pellet was washed with 75% ethanol (subsequently removed by centrifugation at 7,500 x g for 5 minutes at 4 °C), air-dried, and dissolved in RNase/DNase free water (Gibco). The overall purity of RNA was determined with a NanoDrop ND-1000 spectrophotometer (NanoDrop, ThermoScientific), considering the ratio of absorbance at A260/A280 above 1.6 for all the isolated RNA samples. The cDNA synthesis was performed with a total RNA of 1 µg in a volume of 20 µL, which was then diluted 1:10 for the qPCR reactions (3 µL).

The primers used for quantification of the transcripts were pre-designed with PerlPrimer v1.1.21 software (Table S4) and synthesized by MWG Biotech.

Table S4. Primers used for real time RT-PCR.

Target	NCBI reference	Sequence 5' -3'
ACTB	AK223055	F: CTGGAACGGTGAAGGTGACA R: AAGGGACTTCCTGTAACAA
COL1A1	NM_000088.3	GCCAAGACGAAGACATCCCA GGCAGTTCTTGGTCTCGTCA
COL3A1	NM_000090.3	CCTGAAGCTGATGGGGTCAA CAGTGTGTTTCGTGCAACCAT
DCN	NM_001920.4	CACAAGTTTCCTGGGCTGGA AGATGGCATTGACAGCGGAA
SCX	NM_001080514.2	CAGACGGACGTACAGACAGG CAGCGCAGAAAGTTCCAGTG
TNC	NM_002160.3	ACTGCCAAGTTCACAACAGACC CCCACAATGACTTCCTTGACTG
TNMD	NM_022144.2	CCGCGTCTGTGAACCTTTAC CACCCACCAGTTACAAGGCA
IL4	NM_000589.3	GCACCGAGTTGACCGTAACA AGGAATTCAAGCCCGCCAG
IL6	NM_000600.4	AGGAGACTTGCCTGGTGAAA GCATTTGTGGTTGGGTCAG
IL10	NM_000572.2	AAGACCCAGACATCAAGGCG AATCGATGACAGCGCCGTAG
COX2	NM_000963.3	ATGGGGTGATGAGCAGTTGT GAAAGGTGTCAGGCAGAAGG
ACAN	NM_013227.3	TAGAGTCCTCAAGCCTCCTGT TGGTCTGCAGCAGTTGATTC
RUNX2	NM_001024630	TTCCAGACCAGCAGCACTC CAGCGTCAACACCATCATTC
MMP1	NM_002421.3	ACCTGGAAAAATACTACAACCTGAA TTCAATCCTGTAGGTCAGATGTGTT
MMP2	NM_002422.4	GCTACGATGGAGGCGCTAAT TCAGGTATTGCACTGCCAACT
MMP3	NM_002422.4	CACTCACAGACCTGACTCGG AGTCAGGGGGAGGTCCATAG
TIMP1	NM_003254.2	CATCCGGTTCGTCTACACCC GGATAAACAGGGAAACACTGTGC

References

1 P. Dhar, A. Kumar and V. Katiyar, *ACS Appl. Mater. Interfaces*, 2016, **8**, 18393–18409.

2 M. Mahdavi, M. Bin Ahmad, M. J. Haron, F. Namvar, B. Nadi, M. Z. Ab Rahman and J. Amin, *Molecules*, 2013, **18**, 7533–7548.

3 P. Scherrer, *Nachrichten von der Gesellschaft der Wissenschaften - Math. Klasse*, 1918, **2**, 98–100.

4 D. Bondeson, A. Mathew and K. Oksman, *Cellulose*, 2006, **13**, 171–180.

5 R. M. A. Domingues, S. Chiera, P. Gershovich, A. Motta, R. L. Reis and M. E. Gomes, *Adv. Healthc. Mater.*, 2016, **5**, 1364–1375.

6 L. Chen, Q. Wang, K. Hirth, C. Baez, U. P. Agarwal and J. Y. Zhu, *Cellulose*, 2015, **22**, 1753–1762.

7 S. Araújo-Custódio, M. Gomez-Florit, A. R. Tomás, B. B. Mendes, P. S. Babo, S. M. Mithieux, A. S. Weiss, R. Domingues, R. L. Reis and M. E. Gomes, *ACS Biomater. Sci. Eng.*, 2019, **5**, 1392–1404.

8 Z. Shi, J. Tang, L. Chen, C. Yan, S. Tanvir, W. A. Anderson, R. M. Berry and K. C. Tam, *J. Mater. Chem. B*, 2015, **3**, 603–611.

9 H. Lee, S. M. Dellatore, W. M. Miller and P. B. Messersmith, *Science (80-.).*, 2007, **318**, 426–430.